nanomaterials

MDPI

Article

Green Preparation of Fluorescent Nitrogen-Doped Carbon Quantum Dots for Sensitive Detection of Oxytetracycline in Environmental Samples

Rong Gao [1,2,†], Zhibin Wu [1,2,†], Li Wang [2], Jiao Liu [2], Yijun Deng [2], Zhihua Xiao [2], Jun Fang [1,2,*] and Yunshan Liang [1,2,*]

1 Hunan Engineering Laboratory for Pollution Control and Waste Utilization in Swine Production, College of Bioscience and Biotechnology, Hunan Agricultural University, Changsha 410128, China; gaorong0130@163.com (R.G.); wzbaaa11@hunau.edu.cn (Z.W.)

2 Hunan Provincial Key Laboratory of Rural Ecosystem Health in Dongting Lake Area, College of Resources and Environment, Hunan Agricultural University, Changsha 410128, China; wliiris1024@163.com (L.W.); liujiao913@163.com (J.L.); dengyijun9910@163.com (Y.D.); xiaozhihua@hunau.edu.cn (Z.X.)

* Correspondence: fangjun1973@hunau.edu.cn (J.F.); lyss3399@126.com (Y.L.); Tel.: +86-731-8461-3600 (J.F.)

† These authors contributed equally to this work.

Received: 7 July 2020; Accepted: 2 August 2020; Published: 8 August 2020

Abstract: Nitrogen-doped carbon quantum dots (N-CQDs) with strong fluorescence were prepared by a one-step hydrothermal method using natural biomass waste. Two efficient fluorescent probes were constructed for selective and sensitive detection of oxytetracycline (OTC). The synthesized N-CQDs were characterized by UV-visible absorption spectra, fluorescence spectra, Fourier transform infrared spectroscopy (FT-IR), X-ray photon spectroscopy (XPS), atomic force microscopy (AFM), and high-resolution transmission electron microscopy (HRTEM), which proved that the synthesized N-CQDs surface were functionalized and had stable fluorescence performance. The basis of N-CQDs detection of OTC was discussed, and various reaction conditions were studied. Under optimized conditions, orange peel carbon quantum dots (ON-CQDs) and watermelon peel carbon quantum dots (WN-CQDs) have a good linear relationship with OTC concentrations in the range of 2–100 μmol L^{-1} and 0.25–100 μmol L^{-1}, respectively. ON-CQDs and WN-CQDs were both successfully applied in detecting the OTC in pretreated tap water, lake water, and soil, with the recovery rate at 91.724–103.206%, and the relative standard deviation was less than 5.35%. The results showed that the proposed N-CQDs proved to be green and simple, greatly reducing the detection time for OTC in the determination environment.

Keywords: nitrogen-doped carbon quantum dots; natural biomass; fluorescence; oxytetracycline; detection

1. Introduction

Antibiotics are natural, synthetic, or semisynthetic compounds that interfere with the development of other living cells [1]. The global consumption of antibiotics continues to increase, mainly due to the increase in the use of drugs and the demand for animal protein due to the increase in population [1,2]. Oxytetracycline (OTC) is a popular growth accelerator for livestock and aquaculture because of its low cost and strong antibacterial activity [3,4], while it can stay in edatope for more than one year, which is longer than other types of antibiotics [5]. Previous studies have shown that the OTC median in raw sludge was higher than 10 μg kg^{-1} dry matter [6], and the highest TC concentration detected in agricultural soils was 0.6 mg kg^{-1} [7,8]. While the OTC in Honghu, China, had a maximum

concentration of 2796.6 ng L^{-1} [9]. In addition, the comparisons in animal excrement data showed that OTC was consistently the highest average compound [10]. Even more worryingly, antibiotic resistance genes caused by overuse of antibiotics can be transferred between environmental bacteria and human pathogens [11]. While the soil is an important reservoir of antibiotic resistance genes in the environment, resistance genes can be transferred to groundwater or lakes by leaching [12,13]. The amount of antibiotics discharged from pharmaceutical factories, hospitals, and farms in the environment has reached mg L^{-1} level [2,14]. Therefore, it was very necessary to detect antibiotics in the environment, which can effectively identify the residual concentration of antibiotics, improve the detection efficiency, and shorten the detection time, thus indirectly accelerating the pollution prevention and control process.

To date, approaches for detection of OTC mainly include liquid chromatography-tandem mass spectrometry (LC-MS/MS) [15], semiquantitative lateral flow assay (LFA) [16], chemiluminescence [17], as well as enzymatic catalysis [18]. These methods have high stability and sensitivity; however, their applications remain limited due to the complex requirements of expensive equipment and experimental operations [19]. Actually, fluorescence analysis has the advantages of high sensitivity, low cost, and simple operation, which has aroused great interest in the detection field [20–22]. Moreover, the fluorescence method can be applied to the detection of various organic pollutants and metal ions in the environment, including antibiotics (OTC [3], tetracycline [23,24], chlortetracycline [24], enrofloxacin [25]), metal ions (Au^{3+} [26], Hg^{2+} [27,28], Fe^{3+} [24,29,30]), pesticides [31,32] 2,4,6 trinitrophenol [33,34], glutathione [35,36], and chitosan [37].

Carbon quantum dots (CQDs) are a kind of nano-sized spherical carbon fluorescent material with unique advantages of light stability and sensitivity [30,38,39]. So far, different types of biomass materials, including lycium [40], hair [27], sugarcane bagasse pulp [41], Citrus limon peels [42], orange juice [28], tobacco [43], watermelon juice [30], corn juice [44], and carica papaya juice [45] have been used to synthesize CQD. Biowaste was seen as a potential substitute for certain chemicals and waste peels contain carbohydrates, such as fructose, glucose, sucrose, and cellulose [46]. Chatzimitakos et al. synthesized two kinds of CQDs with similar properties from Citrus sinensis and Citrus limon peels using a carbonization process. The results showed that the correlation detection performance of the two kinds of CQDs synthesized from different peels were different, which may be because of their unique analytical properties, which supported their differences [42]. Furthermore, several nitrogenous materials, including rice residue and xylan, have been used to prepare N-CQD to detect antibiotics [23,24]. Using rice residue and glycine as carbon and nitrogen sources, Qi et al. [24] synthesized N-CQD with high quantum yield through one-step hydrothermal method, and this N-CQD was used as a fluorescent probe for the detection of Fe^{3+}, tetracycline, OTC, and aureomycin in actual water samples and cell imaging. The results of the above studies indicated that N-CQD showed excellent solubility, sensitive selectivity, high stability, and good biocompatibility. However, the reaction time of nitrogen doping up to 12 h was more time-consuming and complex, which was not conducive to experimental operation. Yang et al. [23] could synthesize N-CQD with xylan ammonia solution as the precursor in only 10 min, which had excellent photoluminescence properties and a high tolerance to salt and metal ions. Due to the internal filter effect, N-CQD showed high selectivity and sensitivity to tetracycline antibiotics. However, the extraction of xylan was more complex than using common biomass materials, and the purity and stability requirements were higher. The xylan in Yang et al. was purchased from the company. It was proved that the direct preparation of N-CQD by hydrothermal method was an effective method to improve the quality of CQD [47,48]. Heteroatomic doping of CQD not only improves fluorescence efficiency but also provides active sites in CQD to expand its potential applications in analysis and sensing [24]. Through the synergistic coupling effect, heteroatom-doped carbon materials can produce unique electronic structures with higher active sites [49,50]. In particular, nitrogen doping plays an important role in the regulation of electronic and chemical properties of carbon materials. Carbon atoms are replaced by nitrogen to produce posture and induce *n*-type

conductivity [51,52]. Some studies have shown that the density and bonding configuration of dopants can change the physical properties, such as electron and magnetic properties [52].

In this study, waste orange peel and watermelon peel with high carbohydrate content were used as a green carbon source for N-CQDs preparation via a one-step hydrothermal method in ammonia solution. This was a simple green chemical method for preparing large-scale fluorescent carbon dots. The N-CQDs were characterized systematically and the basic conditions for detection of OTC were discussed. Ultimately, synthetic N-CQDs were used for OTC detection in tap water, lake water, and soil treatment samples.

2. Experimental

2.1. Reagents and Chemicals

The OTC standard (95%) was purchased from Aikeda chemical reagent Co. Ltd. (Chengdu, China). The chemical structure of OTC is shown in Figure S1. Ammonia, phosphoric acid, boric acid, acetic acid, sodium hydroxide (NaOH), and anhydrous ethanol were purchased from Sinopharm Chemical Reagent Co. Ltd. (Shanghai, China). All chemicals used were of analytical reagent grade. Britton-Robinson (BR)buffer solution was prepared by a 0.04 mol L^{-1} solution of boric acid, phosphoric acid, and acetic acid (mixed at a ratio of 1:1:1), and the pH value was adjusted to 2–12 with 0.2 mol L^{-1} NaOH solution. The experiment was produced using ultrapure water (Kertone, Changsha, China) with an initial resistivity of 18.25 MΩ.

2.2. Preparation of N-CQDs

Oranges (navel oranges) and watermelons (desert melons in Ningxia) were purchased from fruit stores. The fresh peel (orange peel and watermelon peel) were cut into pieces and dried at 80 °C until the water was completely removed. Then, the sample was broken with a crusher, and the fine particles were selected by using a standard screen (400 mesh) 3 times. We added 0.03 g of orange peel or watermelon peel powder to the lined beaker, then 3 mL of ammonia water and 17 mL of deionized water in this order. After mixing and stirring them, they were put into a tetrafluoroethylene liner beaker and then transferred to a reaction kettle. Orange peel powder was heated at 100 °C for 5 h, and watermelon peel powder was heated at 140 °C for 2 h. After cooling to room temperature, pale yellow solutions were obtained. After centrifugation (10,000 rpm, 10 min), the supernatant was taken and the large particles were removed by 0.22 μm ultrafiltration. The dialysis was then performed under a 500-molecular-weight dialysis bag for two days with the water changed every 2 h. From this, the reserve orange peel nitrogen carbon doped quantum (ON-CQDs) and watermelon peel nitrogen carbon doped quantum dots (WN-CQDs) were obtained.

2.3. Characterization of N-CQDs

The morphologies and sizes of N-CQDs were characterized by transmission electron microscopy (TEM, Tecnai G2 F20, FEI, Hillsborough, Oregon, USA) and multimode V atomic force microscopy (AFM, Veeco, Plainview, NY, USA). TEM and high-resolution transmission electron microscopy (HRTEM, FEI, Hillsborough, Oregon, USA) was scanned at 200 kV. The aqueous solution of the N-CQDs sample was dropped on a 300 mesh ultra-thin carbon coated copper mesh, and then the copper mesh was dried in a vacuum drying box for measurement. The obtained TEM images were analyzed and processed using Gatan Digital Micrograph software. The multifunctional imaging electron spectrometer (XPS, Thermo, Waltham, MA, USA) was collected using a monochromatic Al KaXray source (hv = 1486.6 eV) with a power of 150 W and a beam spot of 500 μm, and its binding energy was calibrated at C1s 284.8. The measurement range of FTIR spectrum was 500–4000 cm^{-1}. The sample liquid was ground together with potassium bromide and measured after being tableted and dried. For F-7000 fluorescence spectrometric measurements (Hitachi High Technologies, Tokyo, Japan), excitation and emission slits were set at 5 nm, and the excitation light-source wavelengths

were set at 320 nm (ON-CQDs) and 280 nm (WN-CQDs). The fluorescence quantum yield of N-CQDs was determined by absolute method (also known as absolute quantum yield) [53–55]. Time-resolved fluorescence decay curve measurements were also performed on the FLS980 series of fluorescence spectrometers (Edinburgh Instruments, Livingston, UK).

2.4. Pretreatment and Preparation of Environmental Samples

Samples of tap water, lake water, and soil were taken from the university campus. Tap water samples were obtained in the laboratory, and lake water samples were collected in front of the laboratory building. The water sample was first settled naturally for 24 h, and then the suspended particles in the lake were filtered with a filter paper with a maximum aperture of 15–20 μm. The filtered water samples were centrifuged at 10,000 rpm for 20 min, and the supernatant was collected and stored in a refrigerator at 4 °C for later use. Soil sampling was carried out by removing the surface soil about 1–2 cm with a scraper, and soil samples were collected rapidly in the new soil section. The samples were naturally air-dried for 48 h and then dried in an oven at 100 °C. The fine particles were selected by using a standard screen (400 mesh) 3 times, and then the dried soil samples were crushed and weighed accurately 1 g. The samples were placed in a hermetically sealed centrifuge tube, followed by mechanical oscillation of 4 mL acetonitrile for 30 min, centrifugation with 5000 r min^{-1} for 10 min, and the supernatant was collected and stored in the centrifuge tube at 4 °C. All standby samples were filtered using a 0.22 μm microporous membrane.

3. Results and Discussion

3.1. Morphologies of N-CQDs

The size and morphology of the synthesized CQDs were analyzed by transmission electron microscopy (TEM) and high-resolution transmission electron microscopy (HRTEM). TEM results showed that both types of N-CQDs had good uniformity and dispersed, and the average particle size was 5 ± 0.5 nm. HRTEM images of ON-CQDs and WN-CQDs were shown in Figure 1a and c, respectively, indicating that ON-CQDs lattice spacing was 0.206 nm and WN-CQDs lattice spacing was 0.208 nm, which was consistent with the (100) plane spacing of sp^2 carbon [56–58]. The particle size distribution diagrams were shown in Figure 1b and d. It can be found that the microscopic morphology of the two N-CQDs were similar. The particle size distribution of both N-CQDs range from 4 to 10 nm, with the maximum distribution at 4 nm. Figure 2 shows the low-magnification images were 5, 20 μm (Figure 2 a and c) and high-magnification images were 2 μm (Figure 2 b and d) of 2D AFM of N-CQDs, which were selected according to the sample morphology [41,59]. It can be seen that acceptable N-CQDs' distribution was obtained in terms of size and shape. Consistent with the TEM results, it was observed that N-CQDs were small, spherical, and the surface roughness was less than 5 nm.

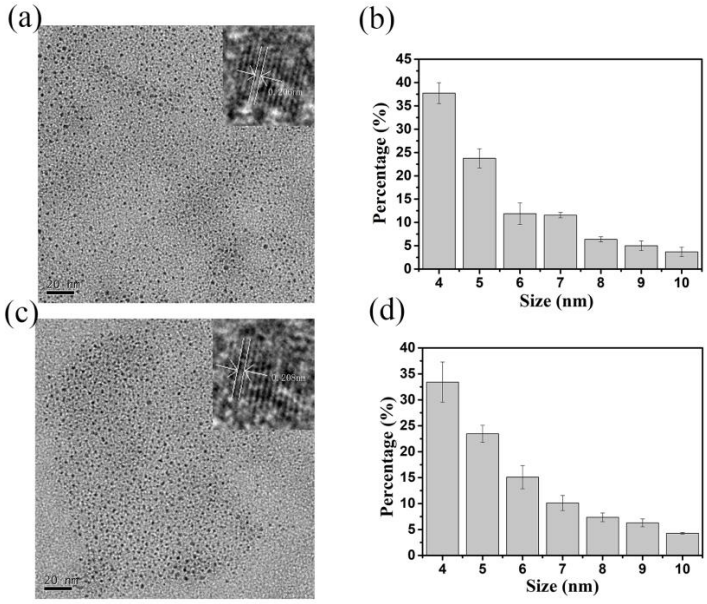

Figure 1. Transmission electron microscopy (TEM) image of the nitrogen-doped carbon quantum dots (N-CQDs). (**a**) orange peel nitrogen carbon doped quantum (ON-CQDs), (**c**) watermelon peel carbon quantum dots (WN-CQDs); (inset: high-resolution transmission electron microscopy (HRTEM) of the N-CQDs); (**b**) and (**d**) shows the size distribution of the carbon dots corresponding to (**a**) and (**c**), respectively.

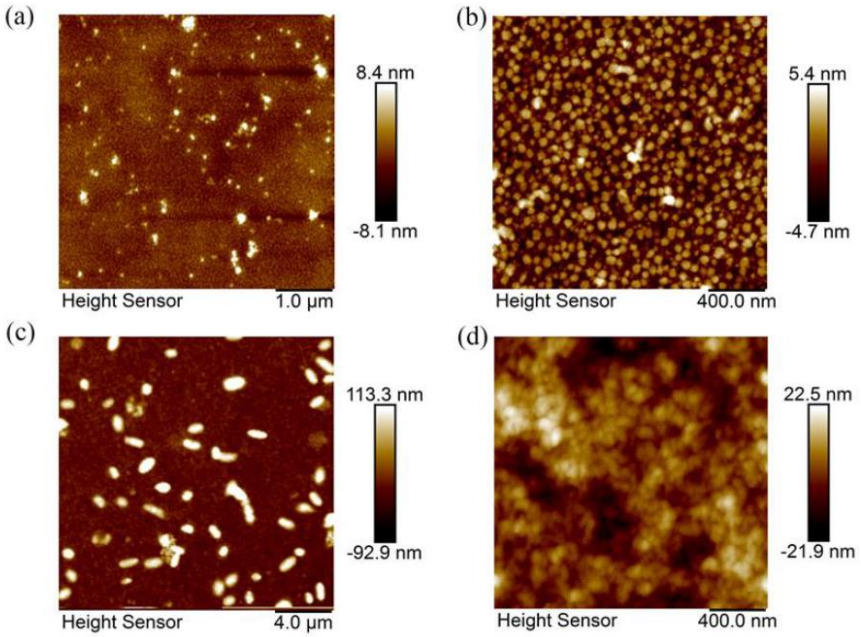

Figure 2. Atomic force microscope (AFM) images of N-CQDs. Low-magnification images of N-CQDs: (**a**) ON-CQDs (5 µm) and (**c**) WN-CQDs (20 µm). (**b**,**d**) are high-magnification images (2 µm) of ON-CQDs and WN-CQDs, respectively.

3.2. Composition of N-CQDs

XPS analysis shows the elemental composition, chemical state, and molecular structure of N-CQDs. The XPS survey spectrum showed that the peaks were 284.79, 399.02, and 531.10 eV in Figure 3a (ON-CQDs) and 285.05, 399.12, and 531.59 eV in Figure 3e (WN-CQDs), corresponding to C1s, N1s, and O1s electrons, respectively. The high-resolution spectrum of the C1s signal shows three peaks at

283.97, 285.42, 287.12 eV (Figure 3b) and 284.10, 285.57, 287.26 eV (Figure 3f), representing the C-C/C=C, C-N/C-O, and C=O groups, respectively [60]. The O1s spectrum (Figure 3c and g) shows two fitting peaks at 530.57, 531.82 eV, and 530.52, 531.87 eV, belonging to C=O and C-O groups, respectively. The high-resolution spectrum of N1s shows two peaks at 399.11, 399.3 eV (Figure 3d) and 399.14, 399.87 eV (Figure 3h), which can be designated as C-N-C and C_2-N-H functional groups, respectively, indicating successful nitrogen doping into CQDs [61,62].

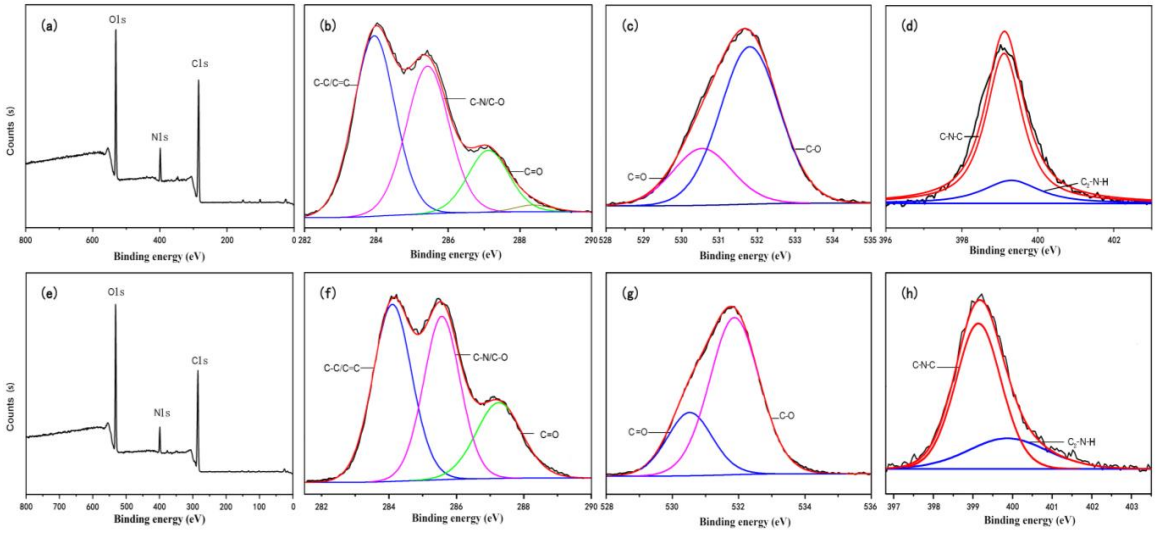

Figure 3. XPS characterizations of N-CQDs. Full spectrum: (**a**,**e**); Cls: (**b**,**f**); Ols: (**c**,**g**); Nls: (**d**,**h**), represents ON-CQDs and WN-CQDs, respectively.

In addition, FTIR spectra were employed to confirm the existence of functional groups. As shown in Figure 4, the peaks at 3354 cm^{-1} and 3339 cm^{-1} could be attributed to the characteristic absorption of O-H by tensile vibration, while the peaks of C=O and C=N are at 1637 cm^{-1} and 2075 cm^{-1}, 2048 cm^{-1}. Meanwhile, the peaks at 1250 cm^{-1} were attributed to the C–N out-of-plane bending vibration [57]. Furthermore, the N-CQDs produced here contain characteristic functional groups, such as -COOH, -OH, and -C-N-C, and all of the data show that it was consistent with XPS [43].

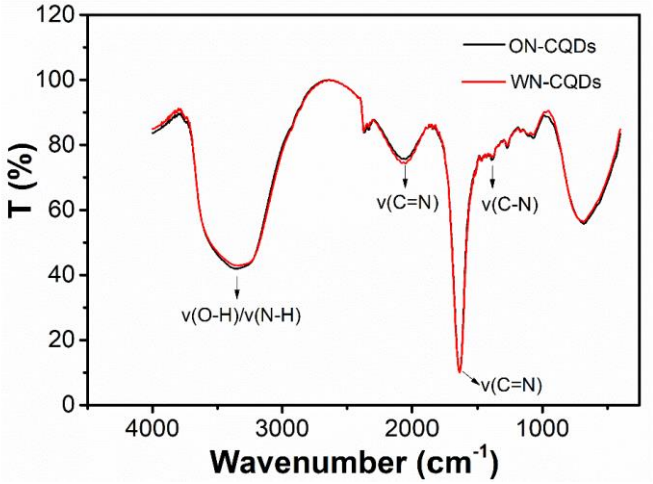

Figure 4. FTIR spectrum of ON-CQDs (black) and WN-CQDs (red).

3.3. Optical Properties of N-CQDs

The optical properties of the prepared N-CQDs were analyzed by UV-visible spectroscopy and fluorescence spectrum. The samples were diluted to 0.2 ± 0.05 mg/mL with deionized water. In the

UV−vis absorption spectrum (Figure 5), ON-CQDs and WN-CQDs presented two obvious absorption peaks at around 265 and 280 nm, respectively. The peaks at 265 and 280 nm were ascribable to the π–π* transition for the C=C or C=O bond in which the orbital was sp^2 hybridized clusters [24,26,27,63]. The fluorescence emission spectra of N-CQDs under different excitations were shown in Figure 6. When the wavelength of the excitation light increased from 250 to 400 nm, the emission peaks were all redshifted. In particular, the excitation wavelength of ON-CQDs produces a corresponding blue shift in the peak position of the emission spectrum at 270 nm and 280 nm. This may be due to the increase in the band gap, and the band gap transition can regulate the fluorescence variation of ON-CQDs [43]. Studies have shown that the nitrogen-doping process can lead to significant redshift of the optimal excitation wavelength and the strongest emission peak, which may depend on the different sizes of distribution of N-CQDs and the characteristics of multi-surface emission points. [26,29,64]. The maximum excitation wavelengths (λ_{ex}) of ON-CQDs (Figure 6a) and WN-CQDs (Figure 6b) were 320 nm and 280 nm, respectively. Studies have also shown that excitation-related emission behaviors may be attributed to the presence of different functional groups to determine the degree and nature of aggregation [44,65].

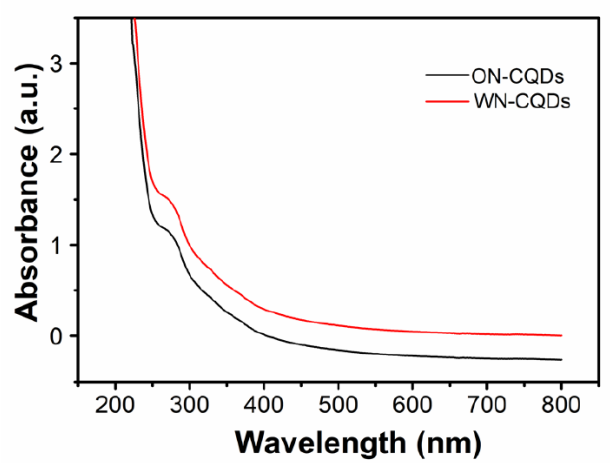

Figure 5. UV-Vis spectrum of ON-CQDs (black) and WN-CQDs (red).

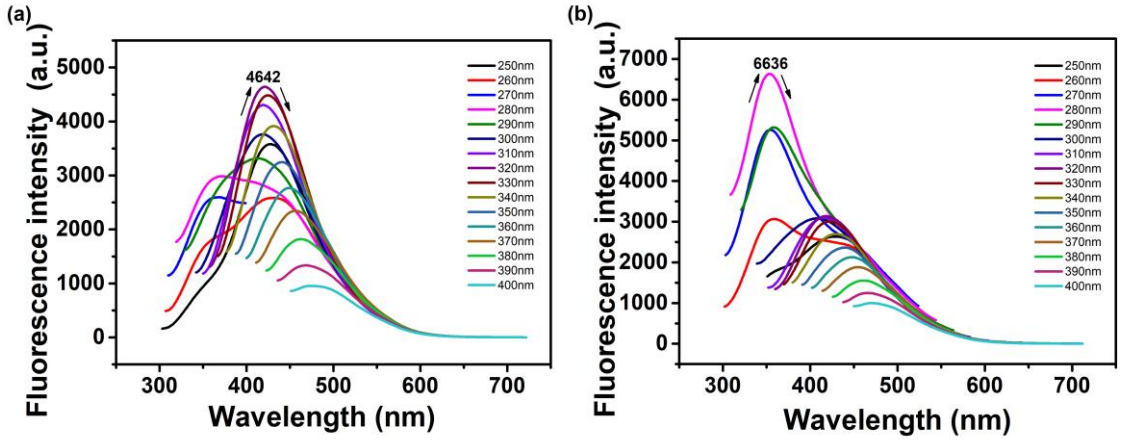

Figure 6. Excitation-dependent fluorescence emission spectra of N-CQDs: (**a**) ON-CQDs; (**b**) WN-CQDs.

The time-resolved fluorescence decay curve, as shown in Figure 7, uses the formula ($f(t) = a_1e^{-t/\tau_1} + a_2e^{-t/\tau_2}$ *with* $a_1 + a_2 = 1$), fitting to a double-exponential decay model function, where τ_1, τ_2 are the fast and slow lifetime components, and a_1, a_2 are the corresponding amplitudes [66]. The change of fluorescence intensity of N-CQDs was a gradual attenuation process, and there were two fluorescent groups in N-CQDs, respectively. The two fluorescence lifetimes indicate the existence of different

luminous states, which indicates that the surface morphology of N-CQDs were not uniform, and there were multiple luminous structures, showing the characteristics of excitation dependence and multiple fluorescence lifetimes [67]. The fluorescence lifetimes of the two fluorophores in ON-CQDs (Figure 7a) were 0.54 ns and 2.95 ns, and the relative concentrations were 29.78% and 70.22%, respectively; the fluorescence lifetimes of the two fluorophores in WN-CQDs (Figure 7b) were 0.56 ns and 2.79 ns, and the relative concentrations were 43.19% and 56.81%, respectively. According to literature, the shorter lifetime comes from surface-related recombination, which was easily affected by the size of N-CQDs and its surface chemistry [68,69]. The fitting results of N-CQDs were comprehensively observed, and it was found that both of them contained a fluorescence lifetime around 0.5 ns and 2.8 ns. It can be inferred that both types of N-CQDs have fluorophores corresponding to this lifetime or different structures of the same fluorescent substance, and the fluorophores corresponding to 2.95 ns and 2.79 ns with a long fluorescence life account for a relatively large contribution rate in the whole decay process. The absolute quantum yields of ON-CQDS and WN-CQDS were calculated as 6.86% and 7.53%, respectively.

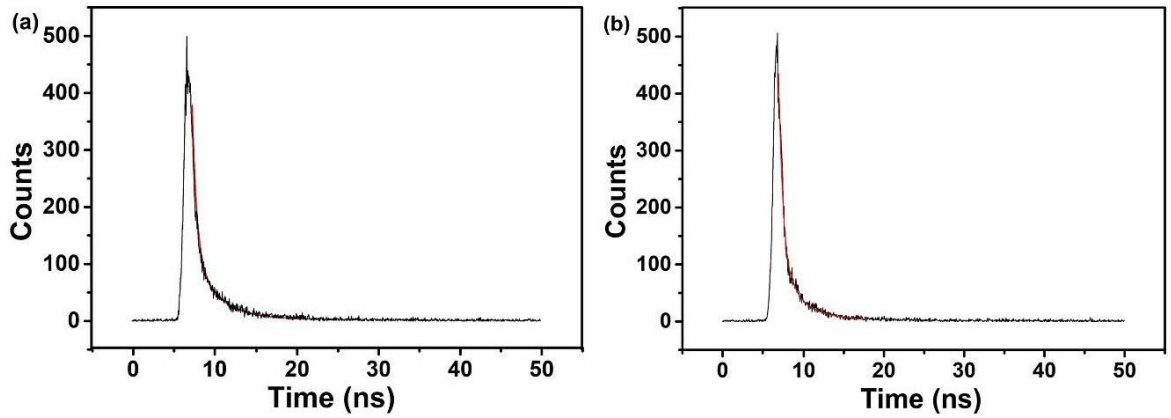

Figure 7. Fluorescence attenuation curve and fitting results: (**a**) ON-CQDs; (**b**) WN-CQDs.

3.4. Basis of OTC Detection

In order to obtain the best detection performance, several key factors affecting the sensitivity and stability of the experiment were studied, such as the pH value of the BR buffer solution (Figure S2), the volume of the BR buffer solution (Figure S3a,b), the order of reagent addition (Figure S4a,b), and the different reaction times (Figure S5). The results showed the best quenching effect on ON-CQDs when the concentration of OTC was 40 μmol L^{-1}, the order of addition was OTC+BR + ON-CQDs, the BR buffer was 1 mL with a pH value of 10, and the incubation time was 20 min. The quenching effect was best when the concentration of OTC was 80 μmol L^{-1}, and the BR buffer was 3 mL with a pH value of 8. The order of adding was OTC + WN-CQDs + BR, which basically stabilized at 20 min.

To investigate the fluorescence quenching of N-CQDs, OTC was added to N-CQDs to form an N-CQDs + OTC composite system. After 20 min, the emission spectra of N-CQD, N-CQDs + OTC, and CK (N-CQDs + deionized water) were measured, respectively. As shown in Figure 8a (ON-CQDs) and b (WN-CQDs), the fluorescence intensity of N-CQDs decreased slightly after the addition of deionized water, which was due to the dilution of the N-CQDs solution. OTC was added to the N-CQDs solution to form the N-CQDs + OTC system, and the fluorescence of N-CQDs fluorescence significantly decreased by about 50%. This was due to the presence of -NH_2 in N-CQDs, which has the fluorescence resonance energy transfer with electron-deficient aromatic rings in the OTC structure, which was consistent with the mechanism reported in the literature [70]. Additionally, the good selectivity results of ON-CQDs (Figure S6a) and WN-CQDs (Figure S6b) were shown in Figure S6, respectively.

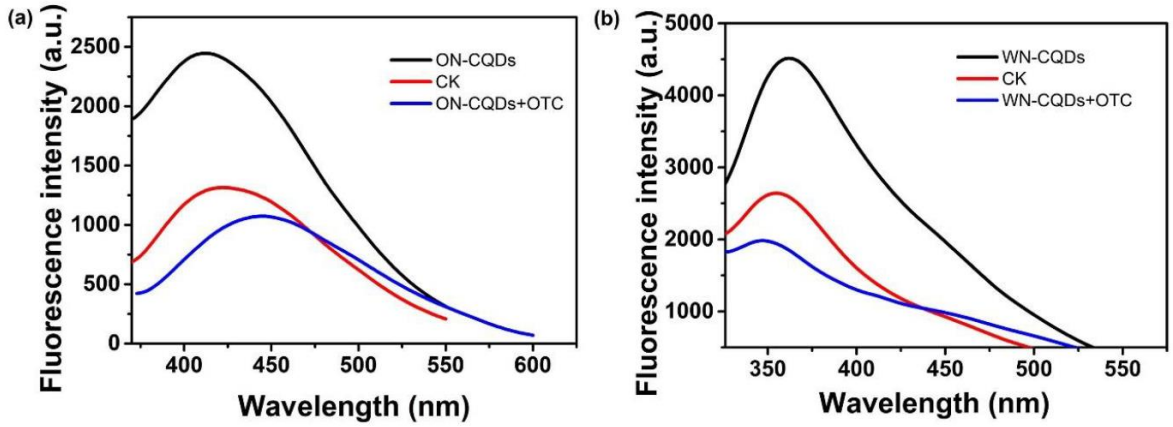

Figure 8. Fluorescence emission spectra of N-CQDs, CK (N-CQDs + deionized water), N-CQDs + OTC. (**a**) ON-CQDs (λ_{ex} = 320 nm); (**b**) WN-CQDs (λ_{ex} = 280 nm).

3.5. Linear Range and Detection Limit of OTC

The sensitivity of N-CQDs to OTC measurement was measured under optimized experimental conditions (Figure 9). Fluorescence intensity difference ($\Delta F = I' - I'_0$) decreases with the increase in OTC concentration, where I′ and I'_0 were, respectively, the fluorescence intensity of N-CQDs in the absence and presence of OTC. ON-CQDs (Figure 9a) and WN-CQDs (Figure 9b), respectively, an OTC concentration of 2–100 μmol L^{-1} and 0.25–100 μmol L^{-1} showed a good linear relationship within the scope of the linear regression equation, respectively, $\Delta F = 0.733\ C(\mu mol\ L^{-1}) + 338.09$ and $\Delta F = 9.2622\ C\ (\mu mol\ L^{-1}) + 358.52$, and the linear correlation coefficient (R^2) were 0.9921 and 0.9903, respectively [71,72]. Furthermore, the detection limit was calculated to be 0.973 μmol L^{-1} (ON-CQDs) and 0.077 μmol L^{-1}(WN-CQDs) based on 3σ/k, where σ and k represent the standard deviation and slope of the curve, respectively. The difference in the detection limit may be caused by the different composition of two N-CQD raw materials. In addition, the analytical performance of this work was compared with the previous detection methods of OTC (Table 1). The results showed that the detection limit of this experiment was lower than most of the reported methods, the linear range was wide, and no complex chemical modification was required.

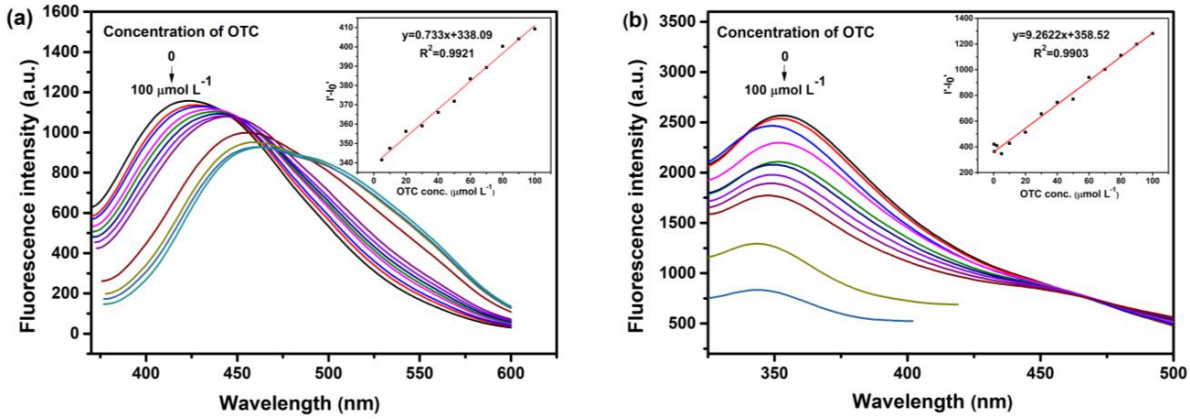

Figure 9. Emission spectra of aqueous N-CQDs dispersion upon addition of various concentrations of OTC. (**a**) ON-CQDs (from top to bottom: 0, 2, 5, 10, 20, 30, 40, 50, 60, 70, 80, 90, and 100 μmol L^{-1}); (**b**) WN-CQDs (from top to bottom: 0, 0.25, 0.5, 2, 5, 10, 20, 30, 40, 50, 60, 70, 80, 90, and 100 μmol L^{-1}). Inset: calibration curve of fluorescence intensity difference with OTC concentration.

Table 1. Comparison with previous methods of OTC analysis.

Method	Linear Range (μmol L^{-1})	Detection Limit (μmol L^{-1})	Citations
N-CQDs fluorescent probe	3.32–32.26	0.3739	[24]
Fluorescent sensor for OTC based on SiNPs	0.2–20	0.18	[4]
Gold nanoclusters fluorescent probe	0.375–12.5	0.15	[73]
BODIPY fluorescent probe	0–42	0.72	[74]
ON-CQDs fluorescent probe	2–100	0.973	This work
WN-CQDs fluorescent probe	0.25–100	0.077	This work

3.6. Determination of OTC in Environmental Samples

Under experimentally optimized conditions, different concentrations of OTC standard solutions were added to pre-treated tap water, lake water, and soil samples and then measured according to the experimental method. Each concentration was measured in parallel five times. As can be seen from Table 2, the recovery of OTC in tap water, lake water, and soil samples were 91.724–103.206%, and the relative standard deviation (RSD) was less than 5.35%. In Table S1, the results were similar and satisfactory to the recoveries of OTC in other samples. It shows that this work can be applied to the detection of antibiotic organic pollutants in the environment.

Table 2. Determination of OTC in environmental samples.

Samples	Spiked	Measured Concentration	Recovery Rate (%)	RSD (%, n = 5)
Lake water [1]	5 μmol L^{-1}	4.870 μmol L^{-1}	97.408	0.62%
Tap water [1]	10 μmol L^{-1}	9.754 μmol L^{-1}	97.544	0.94%
Soil [1]	12.240 μmol Kg^{-1}	12.632 μmol Kg^{-1}	103.206	0.82%
Tap water [1]	30 μmol L^{-1}	27.517 μmol L^{-1}	91.724	1.06%
Lake water [1]	40 μmol L^{-1}	40.341 μmol L^{-1}	100.853	0.62%
Soil [1]	30.600 μmol Kg^{-1}	31.468 μmol Kg^{-1}	102.837	0.88%
Tap water [2]	2 μmol L^{-1}	1.844μmol L^{-1}	92.203	0.84%
Soil [2]	9.180 μmol Kg^{-1}	9.255 μmol Kg^{-1}	100.826	0.81%
Lake water [2]	20 μmol L^{-1}	19.399μmol L^{-1}	96.996	1.05%
Tap water [2]	35 μmol L^{-1}	34.514μmol L^{-1}	98.613	0.94%
Lake water [2]	45 μmol L^{-1}	45.311μmol L^{-1}	100.691	0.88%
Soil [2]	30.600 μmol Kg^{-1}	31.469 μmol Kg^{-1}	102.844	5.35%

Note: sample [1] were ON-CQDs; sample [2] were WN-CQDs.

4. Conclusions

In conclusion, two kinds of N-CQDS were synthesized by a hydrothermal method using waste natural biomass materials (orange peel and watermelon peel) without pre/post chemical treatment. The average particle size at 5 nm of the N-CQDs were both small, both of them contained -COOH, -OH, $-NH_2$, -C-N-C groups, and the fluorescence spectrum was red-shifted as the excitation wavelengths increased. Then, based on the fluorescence quenching responses of N-CQDs, fluorescence probes for OTC detection were successfully constructed with good sensitivity, and detection limits under the optimal reaction conditions were 0.973 μmol L^{-1} (ON-CQDs) and 0.077 μmol L^{-1} (WN-CQDs), respectively. This work was not only environmentally friendly and avoided complex synthetic steps but can also be successfully applied to OTC detection and analysis in the real environment, and it also showed great potential for analyzing trace organic matter in the natural environment.

Supplementary Materials: The following are available online at http://www.mdpi.com/2079-4991/10/8/1561/s1, Figure S1: The chemical structure of OTC, Figure S2: Fluorescence performance of ON-CQDs (black) and WN-CQDs (red) at various pH values, Figure S3: Effect of buffer solution volume on fluorescence intensity of

N-CQDs: (a) ON-CQDs; (b) WN-CQDs, Figure S4: Effect of reagent adding sequence on fluorescence intensity of N-CQDs: (a) ON-CQDs; (b) WN-CQDs, Figure S5: Fluorescence performance of ON-CQDs (black) and WN-CQDs (red) at different reaction times, Figure S6: Selectivity of N-CQDs: (a) ON-CQDs; (b): WN-CQDs. Concentrations of various substances: (a), (b) correspond to 40μmol L^{-1} and 80μmol L^{-1} respectively. (I′ and I'_0 represent the fluorescence intensity of N-CQDs in the presence and absence of various substances, respectively). Table S1: Compare OTC recovery rates in various samples.

Author Contributions: Conceptualization, R.G., Z.W., J.F., and Y.L.; methodology, Z.W., R.G., and Y.L.; validation, Z.W., Z.X., J.F., and Y.L.; formal analysis, R.G., L.W., and J.L.; data curation, R.G., L.W., and Y.D.; writing—original draft preparation, R.G.; writing—review and editing, R.G., J.F., and Y.L.; visualization, J.F. and Y.L.; supervision, Z.W., J.F., and Y.L.; funding acquisition, J.F. and Y.L. All authors have read and agreed to the published version of the manuscript.

Funding: This work was financially supported by the National Natural Science Foundation of China (No.41877491, No.51808215, and No.31672457), the Outstanding Youth Project of Hunan Provincial Department of Education (19B256), Hunan Provincial Science and Technology Department (2018CT5002, 2018WK4025), double first-class construction project of Hunan Agricultural University (SYL201802003, YB2018007, CX20190497).

Conflicts of Interest: The authors declare no conflict of interest.

References

1. Kovalakova, P.; Cizmas, L.; McDonald, T.J.; Marsalek, B.; Feng, M.; Sharma, V.K. Occurrence and toxicity of antibiotics in the aquatic environment: A review. *Chemosphere* **2020**, *251*, 126351. [CrossRef] [PubMed]
2. Zhao, R.X.; Feng, J.; Liu, J.; Fu, W.J.; Li, X.Y.; Li, B. Deciphering of microbial community and antibiotic resistance genes in activated sludge reactors under high selective pressure of different antibiotics. *Water Res.* **2019**, *151*, 388–402. [CrossRef] [PubMed]
3. Liu, H.C.; Ding, L.; Chen, L.G.; Chen, Y.H.; Zhou, T.Y.; Li, H.Y.; Xu, Y.; Zhao, L.; Huang, N. A facile, green synthesis of biomass carbon dots coupled with molecularly imprinted polymers for highly selective detection of oxytetracycline. *J. Ind. Eng. Chem.* **2019**, *69*, 455–463. [CrossRef]
4. Xu, N.; Yuan, Y.Q.; Yin, J.H.; Wang, X.; Meng, L. One-pot hydrothermal synthesis of luminescent silicon-based nanoparticles for highly specific detection of oxytetracycline via ratiometric fluorescent strategy. *RSC Adv.* **2017**, *7*, 48429–48436. [CrossRef]
5. Wu, X.L.; Gu, Y.C.; Wu, X.Y.; Zhou, X.Y.; Zhou, H.; Amanze, C.; Shen, L.; Zeng, W.M. Construction of a tetracycline degrading bacterial consortium and its application evaluation in laboratory-scale soil remediation. *Microorganisms* **2020**, *8*, 292. [CrossRef]
6. Ezzariai, A.; Hafidi, M.; Khadra, A.; Aemig, Q.; Loubna, E.F.; Barret, M.; Merlina, G.; Patureau, D.; Pinelli, E. Human and veterinary antibiotics during composting of sludge or manure: Global perspectives on persistence, degradation, and resistance genes. *J. Hazard. Mater.* **2018**, *359*, 465–481. [CrossRef]
7. Conde-Cid, M.; Fernandez-Calvino, D.; Novoa-Munoz, J.C.; Nunez-Delgado, A.; Fernandez-Sanjurjo, M.J.; Arias-Estevez, M.; Alvarez-Rodriguez, E. Experimental data and model prediction of tetracycline adsorption and desorption in agricultural soils. *Environ. Res.* **2019**, *177*, 108607. [CrossRef]
8. Conde-Cid, M.; Álvarez-Esmorís, C.; Paradelo-Núñez, R.; Nóvoa-Muñoz, J.C.; Arias-Estévez, M.; Álvarez-Rodríguez, E.; Fernández-Sanjurjo, M.J.; Núñez-Delgado, A. Occurrence of tetracyclines and sulfonamides in manures, agricultural soils and crops from different areas in Galicia (NW Spain). *J. Clean. Prod.* **2018**, *197*, 491–500. [CrossRef]
9. Wang, Z.; Du, Y.; Yang, C.; Liu, X.; Zhang, J.Q.; Li, E.H.; Zhang, Q.; Wang, X.L. Occurrence and ecological hazard assessment of selected antibiotics in the surface waters in and around Lake Honghu, China. *Sci. Total Environ.* **2017**, *609*, 1423–1432. [CrossRef]
10. Ghirardini, A.; Grillini, V.; Verlicchi, P. A review of the occurrence of selected micropollutants and microorganisms in different raw and treated manure—Environmental risk due to antibiotics after application to soil. *Sci. Total Environ.* **2020**, *707*, 136118. [CrossRef]
11. Tan, B.; Wang, D.H.; Cai, Z.J.; Quan, X.; Zhao, H.M. Extending suitability of physisorption strategy in fluorescent platforms design: Surface passivation and covalent linkage on MOF nanosheets with enhanced OTC detection sensitivity. *Sens. Actuators B Chem.* **2020**, *303*, 127230. [CrossRef]
12. Zhu, D.; Chen, Q.L.; Ding, J.; Wang, Y.F.; Cui, H.L.; Zhu, Y.G. Antibiotic resistance genes in the soil ecosystem and planetary health: Progress and prospect. *Sci. Sin. Vitae* **2019**, *49*, 1652–1663. [CrossRef]

13. Zhu, Y.G.; Zhao, Y.; Zhu, D.; Gillings, M.; Penuelas, J.; Ok, Y.S.; Capon, A.; Banwart, S. Soil biota, antimicrobial resistance and planetary health. *Environ. Int.* **2019**, *131*, 105059. [CrossRef] [PubMed]
14. Guo, X.Y.; Yan, Z.; Zhang, Y.; Xu, W.L.; Kong, D.Y.; Shan, Z.J.; Wang, N. Behavior of antibiotic resistance genes under extremely high-level antibiotic selection pressures in pharmaceutical wastewater treatment plants. *Sci. Total Environ.* **2018**, *612*, 119–128. [CrossRef]
15. Liang, N.; Huang, P.T.; Hou, X.H.; Li, Z.; Tao, L.; Zhao, L.S. Solid-phase extraction in combination with dispersive liquid-liquid microextraction and ultra-high performance liquid chromatography-tandem mass spectrometry analysis: The ultra-trace determination of 10 antibiotics in water samples. *Anal. Bioanal. Chem.* **2016**, *408*, 1701–1713. [CrossRef]
16. Naik, L.; Sharma, R.; Mann, B.; Lata, K.; Rajput, Y.S.; Surendra Nath, B. Rapid screening test for detection of oxytetracycline residues in milk using lateral flow assay. *Food Chem.* **2017**, *219*, 85–92. [CrossRef]
17. Wang, Y.F.; Xie, T.S.; Yang, J.; Lei, M.; Fan, J.; Meng, Z.H.; Xue, M.; Qiu, L.L.; Qi, F.L.; Wang, Z. Fast screening of antibiotics in milk using a molecularly imprinted two-dimensional photonic crystal hydrogel sensor. *Anal. Chim. Acta* **2019**, *1070*, 97–103. [CrossRef]
18. Hu, Z.T.; Sun, P.D.; Hu, Z.R.; Han, J.Y.; Wang, R.Y.; Jiao, L.; Yang, P.F. Short-term performance of enhanced biological phosphorus removal (EBPR) system exposed to erythromycin (ERY) and oxytetracycline (OTC). *Bioresour. Technol.* **2016**, *221*, 15–25. [CrossRef]
19. Fan, H.Z.; Zhang, M.; Bhandari, B.; Yang, C.H. Food waste as a carbon source in carbon quantum dots technology and their applications in food safety detection. *Trends Food Sci. Technol.* **2020**, *95*, 86–96. [CrossRef]
20. Li, M.; Chen, T.; Gooding, J.J.; Liu, J. Review of carbon and graphene quantum dots for sensing. *ACS Sens.* **2019**, *4*, 1732–1748. [CrossRef]
21. Zhou, J.W.; Zou, X.M.; Song, S.H.; Chen, G.H. Quantum dots applied to methodology on detection of pesticide and veterinary drug residues. *J. Agric. Food Chem.* **2018**, *66*, 1307–1319. [CrossRef] [PubMed]
22. Iravani, S.; Varma, R.S. Green synthesis, biomedical and biotechnological applications of carbon and graphene quantum dots. A review. *Environ. Chem. Lett.* **2020**, *18*, 703–727. [CrossRef] [PubMed]
23. Yang, P.; Zhu, Z.Q.; Chen, M.Z.; Chen, W.M.; Zhou, X.Y. Microwave-assisted synthesis of xylan-derived carbon quantum dots for tetracycline sensing. *Opt. Mater.* **2018**, *85*, 329–336. [CrossRef]
24. Qi, H.J.; Teng, M.; Liu, M.; Liu, S.X.; Li, J.; Yu, H.P.; Teng, C.B.; Huang, Z.H.; Liu, H.; Shao, Q.; et al. Biomass-derived nitrogen-doped carbon quantum dots: Highly selective fluorescent probe for detecting Fe^{3+} ions and tetracyclines. *J. Colloid Interface Sci.* **2019**, *539*, 332–341. [CrossRef] [PubMed]
25. Guo, X.J.; Zhang, L.Z.; Wang, Z.W.; Sun, Y.T.; Liu, Q.S.; Dong, W.; Hao, A.J. Fluorescent carbon dots based sensing system for detection of enrofloxacin in water solutions. *Spectrochim. Acta Part A* **2019**, *219*, 15–22. [CrossRef] [PubMed]
26. Liao, J.; Cheng, Z.H.; Zhou, L. Nitrogen-doping enhanced fluorescent carbon dots: Green synthesis and their applications for bioimaging and label-free detection of Au^{3+} ions. *ACS Sustain. Chem. Eng.* **2016**, *4*, 3053–3061. [CrossRef]
27. Guo, Y.M.; Zhang, L.F.; Cao, F.P.; Leng, Y.M. Thermal treatment of hair for the synthesis of sustainable carbon quantum dots and the applications for sensing Hg^{2+}. *Sci. Rep.* **2016**, *6*, 35795. [CrossRef]
28. Li, Z.L.; Zhang, Y.; Niu, Q.Q.; Mou, M.Y.; Wu, Y.; Liu, X.X.; Yan, Z.Y.; Liao, S.H. A fluorescence probe based on the nitrogen-doped carbon dots prepared from orange juice for detecting Hg^{2+} in water. *J. Lumin.* **2017**, *187*, 274–280. [CrossRef]
29. Zhao, L.; Wang, Y.; Zhao, X.; Deng, Y.; Xia, Y. Facile synthesis of nitrogen-doped carbon quantum dots with chitosan for fluorescent detection of Fe^{3+}. *Polymers* **2019**, *11*, 1731. [CrossRef]
30. Lu, M.C.; Duan, Y.X.; Song, Y.H.; Tan, J.S.; Zhou, L. Green preparation of versatile nitrogen-doped carbon quantum dots from watermelon juice for cell imaging, detection of Fe^{3+} ions and cysteine, and optical thermometry. *J. Mol. Liq.* **2018**, *269*, 766–774. [CrossRef]
31. Wu, M.; Fan, Y.J.; Li, J.W.; Lu, D.Q.; Guo, Y.P.; Xie, L.W.; Wu, Y.Q. Vinyl phosphate-functionalized, magnetic, molecularly-imprinted polymeric microspheres' enrichment and carbon dots' fluorescence-detection of organophosphorus pesticide residues. *Polymers* **2019**, *11*, 1770. [CrossRef] [PubMed]
32. Yang, M.L.; Liu, M.W.; Wu, Z.P.; He, Y.; Ge, Y.L.; Song, G.W.; Zhou, J.G. Carbon dots co-doped with nitrogen and chlorine for "off-on" fluorometric determination of the activity of acetylcholinesterase and for quantification of organophosphate pesticides. *Mikrochim. Acta* **2019**, *186*, 585. [CrossRef] [PubMed]

33. Lai, W.Q.; Guo, J.Q.; Zheng, N.; Nie, Y.J.; Ye, S.; Tang, D.P. Selective determination of 2, 4, 6-trinitrophenol by using a novel carbon nanoparticles as a fluorescent probe in real sample. *Anal. Bioanal. Chem.* **2020**, *412*, 3083–3090. [CrossRef]
34. Wang, M.; Gao, M.J.; Deng, L.L.; Kang, X.; Zhang, K.L.; Fu, Q.F.; Xia, Z.N.; Gao, D. A sensitive and selective fluorescent sensor for 2, 4, 6-trinitrophenol detection based on the composite material of magnetic covalent organic frameworks, molecularly imprinted polymers and carbon dots. *Microchem. J.* **2020**, *154*, 104590. [CrossRef]
35. Ma, Y.; Chen, A.Y.; Huang, Y.Y.; He, X.; Xie, X.F.; He, B.; Yang, J.H.; Wang, X.Y. Off-on fluorescent switching of boron-doped carbon quantum dots for ultrasensitive sensing of catechol and glutathione. *Carbon* **2020**, *162*, 234–244. [CrossRef]
36. Zhu, P.D.; Gan, Y.; Lin, K.P.; Lin, C.; Li, S.S.; Yu, S.L.; Shi, J.H. Dual-response detection of oxidized glutathione, ascorbic acid, and cell imaging based on pH/redox dual-sensitive fluorescent carbon dots. *ACS Omega* **2020**, *5*, 4482–4489. [CrossRef]
37. Pawar, S.; Togiti, U.K.; Bhattacharya, A.; Nag, A. Functionalized chitosan-carbon dots: A fluorescent probe for detecting trace amount of water in organic solvents. *ACS Omega* **2019**, *4*, 11301–11311. [CrossRef]
38. Yu, D.; Wang, L.; Zhou, H.Y.; Zhang, X.J.; Wang, L.; Qiao, N. Fluorimetric detection of *candida albicans* using cornstalk N-carbon quantum dots modified with amphotericin B. *Bioconjug. Chem.* **2019**, *30*, 966–973. [CrossRef]
39. Wang, Y.F.; Hu, A.G. Carbon quantum dots: Synthesis, properties and applications. *J. Mater. Chem. C* **2014**, *2*, 6921. [CrossRef]
40. Hu, Y.F.; Zhang, L.L.; Lin, L.Y.; Li, X.F.; Zhao, S.L.; Liang, H. Preparation of carbon quantum dots from lycium chinensis and as a fluorescent probe for high sensitive detection of *D*-penicillamine. *Sci. Sin. Chim.* **2017**, *47*, 258–266. [CrossRef]
41. Thambiraja, S.; Shankaran, D.R. Green synthesis of highly fluorescent carbon quantum dots from sugarcane bagasse pulp. *Appl. Surf. Sci.* **2016**, *390*, 435–443. [CrossRef]
42. Chatzimitakos, T.; Kasouni, A.; Sygellou, L.; Avgeropoulos, A.; Troganis, A.; Stalikas, C. Two of a kind but different: Luminescent carbon quantum dots from Citrus peels for iron and tartrazine sensing and cell imaging. *Talanta* **2017**, *175*, 305–312. [CrossRef] [PubMed]
43. Miao, H.; Wang, Y.Y.; Yang, X.M. Carbon dots derived from tobacco for visually distinguishing and detecting three kinds of tetracyclines. *Nanoscale* **2018**, *10*, 8139–8145. [CrossRef] [PubMed]
44. Sangubotla, R.; Kim, J. A facile enzymatic approach for selective detection of γ-aminobutyric acid using corn-derived fluorescent carbon dots. *Appl. Surf. Sci.* **2019**, *490*, 61–69. [CrossRef]
45. Kasibabu, B.S.; D'Souza, S.L.; Jha, S.; Kailasa, S.K. Imaging of bacterial and fungal cells using fluorescent carbon dots prepared from *carica papaya* juice. *J. Fluoresc.* **2015**, *25*, 803–810. [CrossRef]
46. Prasannan, A.; Imae, T. One-pot synthesis of fluorescent carbon dots from orange waste peels. *Ind. Eng. Chem. Res.* **2013**, *52*, 15673–15678. [CrossRef]
47. Wang, R.X.; Wang, X.F.; Sun, Y.M. One-step synthesis of self-doped carbon dots with highly photoluminescence as multifunctional biosensors for detection of iron ions and pH. *Sens. Actuators B Chem.* **2017**, *241*, 73–79. [CrossRef]
48. Liu, Y.; Liu, Y.A.; Park, S.J.; Zhang, Y.F.; Kim, T.; Chae, S.; Park, M.; Kim, H.Y. One-step synthesis of robust nitrogen-doped carbon dots: Acid-evoked fluorescence enhancement and their application in Fe^{3+} detection. *J. Mater. Chem. A* **2015**, *3*, 17747–17754. [CrossRef]
49. Wang, X.W.; Sun, G.; Routh, P.; Kim, D.-H.; Huang, W.; Chen, P. Heteroatom-doped graphene materials: Syntheses, properties and applications. *Chem. Soc. Rev.* **2014**, *43*, 7067–7098. [CrossRef]
50. Hung, Y.H.; Dutta, D.; Tseng, C.J.; Chang, J.K.; Bhattacharyya, A.J.; Su, C.Y. Manipulation of heteroatom substitution on nitrogen and phosphorus co-doped graphene as a high active catalyst for hydrogen evolution reaction. *J. Phys. Chem. C* **2019**, *123*, 22202–22211. [CrossRef]
51. Telychko, M.; Mutombo, P.; Ondracek, M.; Hapala, P.; Bocquet, F.; Kolorenc, J.; Vondracek, M.; Jelinek, P.; Svec, M. Achieving high-quality single-atom nitrogen doping of graphene/SiC(0001) by ion implantation and subsequent thermal stabilizatio. *ACS Nano* **2014**, *8*, 7318–7324. [CrossRef] [PubMed]
52. Velez-Fort, E.; Mathieu, C.; Pallecchi, E.; Pigneur, M.; Silly, M.G.; Belkhou, R.; Marangolo, M.; Shukla, A.; Sirotti, F.; Ouerghi, A. Epitaxial graphene on 4H-SiC(0001) grown under nitrogen flux: Evidence of low nitrogen-doping and high charge transfer. *ACS Nano* **2012**, *6*, 10893–10900. [CrossRef] [PubMed]

53. Liu, X.; Pang, J.H.; Xu, F.; Zhang, X.M. Simple approach to synthesize amino-functionalized carbon dots by carbonization of chitosan. *Sci. Rep.* **2016**, *6*, 31100. [CrossRef] [PubMed]
54. Liu, Z.Y.; Mo, Z.L.; Niu, X.H.; Yang, X.; Jiang, Y.Y.; Zhao, P.; Liu, N.J.; Guo, R.B. Highly sensitive fluorescence sensor for mercury(II) based on boron- and nitrogen-co-doped graphene quantum dots. *J. Colloid Interface Sci.* **2020**, *566*, 357–368. [CrossRef]
55. Ma, P.P.; Sun, X.B.; Pan, W.; Yu, G.F.; Wang, J.P. Green and orange emissive carbon dots with high quantum yields dispersed in matrices for phosphor-based white LEDs. *ACS Sustain. Chem. Eng.* **2020**, *8*, 3151–3161. [CrossRef]
56. Lu, J.; Yang, J.X.; Wang, J.Z.; Lim, A.; Wang, S.; Loh, K.P. One-pot synthesis of fluorescent carbon nanoribbons, nanoparticles, and graphene by the exfoliation of graphite in ionic liquids. *ACS Nano* **2009**, *3*, 2367–2375. [CrossRef]
57. Yang, X.M.; Luo, Y.W.; Zhu, S.S.; Feng, Y.J.; Zhuo, Y.; Dou, Y. One-pot synthesis of high fluorescent carbon nanoparticles and their applications as probes for detection of tetracyclines. *Biosens. Bioelectron.* **2014**, *56*, 6–11. [CrossRef]
58. Martindale, B.C.M.; Hutton, G.A.M.; Caputo, C.A.; Reisner, E. Solar hydrogen production using carbon quantum dots and a molecular nickel catalyst. *J. Am. Chem. Soc.* **2015**, *137*, 6018–6025. [CrossRef]
59. Carneiro Cruz, A.A.; Freire, R.M.; Froelich, D.B.; Alves de Lima, A.C.; Muniz, A.R.; Ferreira, O.P.; Fechine, P.B.A. Fluorescence based platform to discriminate protein using carbon quantum dots. *ChemistrySelect* **2019**, *4*, 5619–5627. [CrossRef]
60. Atchudan, R.; Edison, T.N.J.I.; Aseer, K.R.; Perumal, S.; Karthik, N.; Lee, Y.R. Highly fluorescent nitrogen-doped carbon dots derived from *Phyllanthus acidus* utilized as a fluorescent probe for label-free selective detection of Fe^{3+} ions, live cell imaging and fluorescent ink. *Biosens. Bioelectron.* **2018**, *99*, 303–311. [CrossRef]
61. Shi, B.F.; Su, Y.B.; Zhang, L.L.; Huang, M.J.; Liu, R.J.; Zhao, S.L. Nitrogen and phosphorus co-doped carbon nanodots as a novel fluorescent probe for highly sensitive detection of Fe^{3+} in human serum and living cells. *ACS Appl. Mater. Interfaces* **2016**, *8*, 10717–10725. [CrossRef] [PubMed]
62. Murugana, N.; Prakash, M.; Jayakumar, M.; Sundaramurthy, A.; Sundramoorthy, A.K. Green synthesis of fluorescent carbon quantum dots from *Eleusine coracana* and their application as a fluorescence 'turn-off' sensor probe for selective detection of Cu^{2+}. *Appl. Surf. Sci.* **2019**, *476*, 468–480. [CrossRef]
63. Vaz, R.; Bettini, J.; Júnior, J.G.F.; Lima, E.D.S.; Botero, W.G.; Santos, J.C.C.; Schiavon, M.A. High luminescent carbon dots as an eco-friendly fluorescence sensor for Cr(VI) determination in water and soil samples. *J. Photochem. Photobiol. A* **2017**, *346*, 502–511. [CrossRef]
64. Song, Z.Q.; Quan, F.Y.; Xu, Y.H.; Liu, M.L.; Cui, L.; Liu, J.Q. Multifunctional N,S co-doped carbon quantum dots with pH and thermo-dependent switchable fluorescent properties and highly selective detection of glutathione. *Carbon* **2016**, *104*, 169–178. [CrossRef]
65. Sharma, A.; Gadly, T.; Gupta, A.; Ballal, A.; Ghosh, S.K.; Kumbhakar, M. Origin of excitation dependent fluorescence in carbon nanodots. *J. Phys. Chem. Lett.* **2016**, *7*, 3695–3702. [CrossRef]
66. Goreham, R.V.; Schroeder, K.L.; Holmes, A.; Bradley, S.J.; Nann, T. Demonstration of the lack of cytotoxicity of unmodified and folic acid modified graphene oxide quantum dots, and their application to fluorescence lifetime imaging of HaCaT cells. *Mikrochim. Acta* **2018**, *185*, 128. [CrossRef]
67. Becker, W. Fluorescence lifetime imaging-techniques and applications. *J. Microsc.* **2012**, *247*, 119–136. [CrossRef]
68. Li, Q.; Luo, T.Y.; Zhou, M.; Abroshan, H.; Huang, J.; Kim, H.J.; Rosi, N.L.; Shao, Z.; Jin, R. Silicon nanoparticles with surface nitrogen: 90% quantum yield with narrow luminescence bandwidth and the ligand structure based energy law. *ACS Nano* **2016**, *10*, 8385–8393. [CrossRef]
69. Chandra, S.; Ghosh, B.; Beaune, G.; Nagarajan, U.; Yasui, T.; Nakamura, J.; Tsuruoka, T.; Baba, Y.; Shirahata, N.; Winnik, F.M. Functional double-shelled silicon nanocrystals for two-photon fluorescence cell imaging: Spectral evolution and tuning. *Nanoscale* **2016**, *8*, 9009–9019. [CrossRef]
70. Fang, Y.X.; Guo, S.J.; Li, D.; Zhu, C.Z.; Ren, W.; Dong, S.J.; Wang, E.K. Easy synthesis and imaging applications of cross-linked green fluorescent hollow carbon nanoparticles. *ACS Nano* **2012**, *6*, 400–409. [CrossRef]
71. Shen, J.; Zhang, T.; Cai, Y.; Chen, X.Y.; Shang, S.M.; Li, J. Highly fluorescent N, S-co-doped carbon dots: Synthesis and multiple applications. *New J. Chem.* **2017**, *41*, 11125–11137. [CrossRef]

72. Meng, A.; Xu, Q.H.; Zhao, K.; Li, Z.J.; Liang, J.; Li, Q.D. A highly selective and sensitive "on-off-on" fluorescent probe for detecting Hg(II) based on Au/N-doped carbon quantum dots. *Sens. Actuators B Chem.* **2018**, *255*, 657–665. [CrossRef]
73. Xu, S.H.; Li, X.L.; Mao, Y.N.; Gao, T.; Feng, X.Y.; Luo, X.L. Novel dual ligand co-functionalized fluorescent gold nanoclusters as a versatile probe for sensitive analysis of Hg^{2+} and oxytetracycline. *Anal. Bioanal. Chem.* **2016**, *408*, 2955–2962. [CrossRef] [PubMed]
74. Xu, Z.Q.; Yi, X.F.; Wu, Q.; Zhu, Y.C.; Ou, M.R.; Xu, X.P. First report on a Bodipy-based fluorescent probe for sensitive detection of oxytetracycline: Application for the rapid determination of oxytetracycline in milk, honey and pork. *RSC Adv.* **2016**, *6*, 89288–89297. [CrossRef]